

# Approximation of variable density incompressible flows by means of finite elements and finite volumes

Yann Fraigneau<sup>1</sup>, Jean-Luc Guermond<sup>1,\*</sup> and Luigi Quartapelle<sup>2</sup>

<sup>1</sup>*Laboratoire d'Informatique pour la Mécanique et les Sciences de l'Ingénieur, CNRS, BP 133, 91403, Orsay, France*

<sup>2</sup>*Dipartimento di Ingegneria Aerospaziale, Politecnico di Milano, Via La Masa, 34, 20158 Milano, Italy*

## SUMMARY

This work describes a projection method for approximating incompressible viscous flows of non-uniform density. It is shown that unconditional stability in time is possible provided two projections are performed per time step. A finite element implementation and a finite volume one are described and compared. The performance of the two methods are tested on a Rayleigh–Taylor instability. We show that the considered problem has no inviscid smooth limit; hence confirming a conjecture by Birkhoff stating that the inviscid problem is not well-posed. Furthermore, we show that at even moderate Reynolds numbers, this problem is extremely sensitive to mesh refinement and to the numerical method adopted. Copyright © 2001 John Wiley & Sons, Ltd.

KEY WORDS: finite element; finite volume; incompressible viscous flows; Rayleigh–Taylor instability

## 1. INTRODUCTION

Simulating variable density incompressible viscous flows presents the difficulty of satisfying the property of mass conservation in two respects. On the one hand, the mass density of each fluid particle must remain unchanged during the fluid motion, whatever the level of unsteadiness and mixing. On the other hand, the velocity field must satisfy the incompressibility constraint which reflects the inability of pressure to do compression work. These two important physical characteristics are fully described by the set of the incompressible Navier–Stokes equations augmented by the advection equation for the density. These equations are expressed in terms of the primitive variables: density  $\rho$ , velocity  $\mathbf{u}$  and pressure  $P$ . The mathematical statement of the problem is: find  $\rho > 0$ ,  $\mathbf{u}$  and  $P$  up to a constant (actually, up to an arbitrary function of  $t$  only), so that

$$\begin{aligned} \frac{\partial \rho}{\partial t} + \nabla \cdot (\rho \mathbf{u}) &= 0 \\ \frac{\partial (\rho \mathbf{u})}{\partial t} + \nabla \cdot (\rho \mathbf{u} \otimes \mathbf{u}) - \mu \nabla^2 \mathbf{u} + \nabla P &= \mathbf{f} \\ \nabla \cdot \mathbf{u} &= 0 \end{aligned} \tag{1}$$

\*Correspondence to: J.-L. Guermond, Laboratoire d'Informatique pour la Mécanique et les Sciences de l'Ingénieur, CNRS, B.P. 133, 91403, Orsay Cedex, France

where  $\mu > 0$  the (shear) viscosity of the fluid (assumed here to be a constant) and  $\mathbf{f}$  is a known body force (per unit volume), possibly dependent on space, or time, or both; typically, in stratified flows,  $\mathbf{f} = \rho \mathbf{g}$ ,  $\mathbf{g}$  being the gravity field. We recall that  $\nabla \cdot (\rho \mathbf{u} \otimes \mathbf{u}) = \partial_j (\rho u_i u_j)$ . The viscous stress contribution due to bulk viscosity is zero by the assumed incompressibility of the flow.

The complete mathematical statement of the problem requires suitable boundary and initial conditions. For the sake of simplicity, only Dirichlet boundary conditions for velocity are considered here, but more general boundary conditions can be handled by the techniques presented below. We shall assume a homogeneous Dirichlet condition on the velocity on the entire boundary.

$$\rho|_{t=0} = \rho_0, \quad \mathbf{u}|_{t=0} = \mathbf{u}_0, \quad \mathbf{u}|_{\Gamma} = \mathbf{b} \quad (2)$$

where  $\rho_0 > 0$  and  $\mathbf{u}_0$  are the initial distributions of density and velocity, and  $\mathbf{b}$  is the velocity prescribed on the boundary with  $\mathbf{b} \cdot \mathbf{n} = 0$ .

The solvability of the problem defined by equation system (1) supplemented with the boundary and initial conditions (2) requires the satisfaction of the following conditions on the boundary and initial data for the velocity:

$$\int_{\Gamma} \mathbf{n} \cdot \mathbf{b} = 0, \quad \forall t \geq 0, \quad \text{and} \quad \nabla \cdot \mathbf{u}_0 = 0, \quad \mathbf{n} \cdot \mathbf{b}|_{t=0} = \mathbf{n} \cdot \mathbf{u}_0|_{\Gamma} \quad (3)$$

For the mathematical theory of existence and uniqueness of solutions to this set of equations, we refer to Lions [1]. This theory is far from being trivial due to the fact that the equations governing the motion of a variable density but incompressible fluid constitute a mixed PDE system entangling hyperbolic, parabolic and elliptic features.

The variable density incompressible Navier–Stokes equations are important in several fields of fluid dynamics: for instance, in highly stratified flows, in the study of the dynamics of interfaces between fluids of different density, in problems of inertial confinement and in astrophysics.

The goal of the present work is to describe a projection method for approximating the solution to Equations (1) and (2) in the same spirit as that of Chorin [2, 3] and Teman [4, 5]. The paper is organized as follows. In Section 2, we present a projection method and prove that unconditional stability in time is possible provided two projections are performed per time step. We also describe two implementations of the method: one with finite elements and the other with finite volumes. The performance of the two methods are tested in Section 3. The test problem is a Rayleigh–Taylor instability. We show that the considered problem has no inviscid smooth limit, hence confirming a conjecture by Birkhoff stating that the inviscid problem is not well-posed. As a consequence, at high Reynolds numbers or large dimensionless times, this problem is very sensitive to mesh variations and to the numerical method adopted.

## 2. A FINITE ELEMENT METHOD

### 2.1. A projection method for variable density flows

The main idea of the fractional step projection method of Chorin [2, 3] and Teman [4, 5] consists of splitting the viscous effects and the incompressibility. Various extensions of this

technique to variable density flows have been devised, see e.g. Bell and Marcus [6], but to our knowledge, none of them have been shown to yield unconditional stability in time. The objective of this section is to present a second-order accurate projection method that is unconditionally stable.

We adopt the three-level BDF method for marching in time in the mass equation and the momentum equation. To this end, we introduce the linearly extrapolated velocity field at the new time level by means of the definition

$$\mathbf{u}_{\star}^{n+1} = 2\mathbf{u}^n - \mathbf{u}^{n-1} \quad (4)$$

Setting  $\sigma = \sqrt{\rho}$ , the complete set of uncoupled problems to be solved in the BDF incremental projection method assumes the form

$$\frac{3}{2\Delta t}\rho^{n+1} + \mathbf{u}_{\star}^{n+1} \cdot \nabla \rho^{n+1} + \frac{1}{2}(\nabla \cdot \mathbf{u}_{\star}^{n+1})\rho^{n+1} = \frac{4\rho^n - \rho^{n-1}}{2\Delta t} \quad (5)$$

$$\rho_{|\Gamma_{\text{in}}}^{n+1} = a^{n+1}$$

$$-\nabla \cdot \left( \frac{1}{\rho^{n+1}} \nabla P^{n+1} \right) = -\nabla \cdot \left( \frac{1}{\sigma^{n+1}\sigma^n} \nabla Q^n \right) \quad (6)$$

$$\frac{1}{\sigma^{n+1}} \frac{\partial P^{n+1}}{\partial n} \Big|_{\Gamma} = \frac{1}{\sigma^n} \frac{\partial Q^n}{\partial n} \Big|_{\Gamma}$$

$$\begin{aligned} & \frac{3\rho^{n+1}}{2\Delta t} \mathbf{u}^{n+1} - \mu \nabla^2 \mathbf{u}^{n+1} + (\rho^{n+1} \mathbf{u}_{\star}^{n+1} \cdot \nabla) \mathbf{u}^{n+1} + \frac{1}{2} [\nabla \cdot (\rho^{n+1} \mathbf{u}_{\star}^{n+1})] \mathbf{u}^{n+1} \\ &= \frac{2}{\Delta t} \sigma^{n+1} \sigma^n \mathbf{u}^n - \frac{1}{2\Delta t} \sigma^{n+1} \sigma^{n-1} \mathbf{u}^{n-1} + \mathbf{f}^{n+1} \\ & -\nabla P^{n+1} - \frac{4\sigma^{n+1}}{3\sigma^n} \nabla(Q^n - P^n) + \frac{\sigma^{n+1}}{3\sigma^{n-1}} \nabla(Q^{n-1} - P^{n-1}) \end{aligned} \quad (7)$$

$$\mathbf{u}_{|\Gamma}^{n+1} = \mathbf{b}^{n+1}$$

$$-\nabla \cdot \left( \frac{1}{\rho^{n+1}} \nabla(Q^{n+1} - P^{n+1}) \right) = -\frac{3}{2\Delta t} \nabla \cdot \mathbf{u}^{n+1} \quad (8)$$

$$\frac{\partial(Q^{n+1} - P^{n+1})}{\partial n} \Big|_{\Gamma} = 0$$

We refer to Guermond–Quartapelle [7] for details. Note that (6) and (8) are projection steps. Contrary to other known projection methods, the present one contains two projection steps. Given this particularity, the following stability results are established in Reference [7]:

*Theorem 2.1.* For any  $\Delta t > 0$ , the solution  $(\rho^n, \mathbf{u}^n, P^n)$ ,  $n = 1, 2, \dots$ , of the incremental projection method (5)–(8) with  $\mathbf{f} = 0$  satisfies the stability estimate

$$\|\sigma^{n+1} \mathbf{u}^{n+1}\|_0^2 + (\Delta t)^2 \left\| \frac{\nabla Q^{n+1}}{\sigma^{n+1}} \right\|_0^2 + 2\mu\Delta t \sum_{k=0}^n \|\nabla \mathbf{u}^{k+1}\|_0^2 \leq c \left( \|\sigma_0 \mathbf{u}_0\|_0^2 + (\Delta t)^2 \left\| \frac{\nabla Q_0}{\sigma_0} \right\|_0^2 \right)$$

## 2.2. The finite element implementation

We adopt a mixed finite element technique where the density and the velocity are approximated in the same space. This choice makes it very easy to develop the method from an existing FEM solver dedicated to the solution of uniform density flows (see Guermond–Quartapelle [8]). In our implementation, we use  $\mathbb{P}_1$  interpolation for pressure and  $\mathbb{P}_2$  interpolation for velocity and density.

Of course, the solution of the discrete Equation (5) presents well-known difficulties pertaining to any Galerkin finite element approximation to hyperbolic problems. To avoid the spurious spatial oscillations induced by the Galerkin technique, we have used a new stabilization procedure proposed in Reference [9]. This technique basically amounts to introducing a two-level hierarchical decomposition of the finite element space and to adding a non-linear diffusion term to Equation (5) as follows:

$$\left( v_h, \frac{\rho_h^{n+1} - \rho_h^n}{\Delta t} \right) + (v_h, \mathbf{u}_h^n \cdot \nabla \rho_h^{n+1} + \frac{1}{2} (\nabla \cdot \mathbf{u}_h^n) \rho_h^{n+1}) = b_h(v_h, \rho_h^n, \rho_h^n)$$

where  $b_h(v_h, \rho_h, \rho_h)$  is a trilinear form of order  $h^{k+1}$  when  $\rho_h$  is smooth,  $k$  being the order of interpolation of the density. For a detailed description of this subgrid stabilization technique the reader is referred to [9].

The two projection steps (6) and (8) are solved in weak form as Poisson problems. The homogeneous Neumann boundary conditions are enforced naturally by the weak formulation.

## 2.3. A finite volumes method

We now describe a finite volume method developed by the first author.

The conservation equations for mass and momentum are used in conservative form (1) and are discretized on a structured staggered grid.

For the momentum equation, the advection fluxes are estimated following a strategy proposed by Leonard [10]. For each cell face, the fluxes are computed with the Quickest scheme, based on upwind biased cubic interpolation. This scheme derives from the method of characteristics. We recall that the method of characteristics is based on the following property: for pure advection of a scalar  $F$  at constant vector velocity  $V$ , the exact solution at time  $t + dt$  is  $F(x, t + dt) = F(x - Vdt, t)$ . As long as there are no oscillations, we use the method of characteristics after linearization. Otherwise, we use the flux limiter devised in Reference [10] for the Ultimate-Quickest scheme.

To march in time we have adopted a projection method with only one projection step per time step as in Bell and Marcus [6]. The momentum equation is solved in the form of a matrix system arising from an implicit formulation of diffusion fluxes:  $L[V(t + dt)] = S(t)$ .  $S$  is the source term containing pressure gradient, advection fluxes and the explicit contribution of the temporal discretization.  $L$  is the matrix defined by discretization of the diffusion fluxes

and the temporal term associated with  $V(t + dt)$ . The linear systems are solved by means of the ADI algorithm. The pressure Poisson equation is solved by means of a multigrid method.

The mass equation is directly solved following the method of characteristics [11]. The advective fluxes are estimated using either Superbee [12, 13] or Super-C [10]. These schemes are known to be second order and Superbee is TVD. Both succeed in convecting discontinuities without introducing excessive numerical diffusion. The main difference between both schemes is that Super-C is less diffusive than Superbee when convecting a discontinuity. For example, if we consider the convection of a 1D step function, the numerical diffusion smooths the step over 3–4 grid cells for Super-C, whereas it typically spreads from 6 to 7 cells for Superbee. These results depend weakly on the Courant number.

### 3. NUMERICAL RESULTS

#### 3.1. The Rayleigh–Taylor instability

As a test case we have computed the development of a Rayleigh–Taylor instability in the viscous regime. Our starting point is the problem documented by Tryggvason [14]. This problem consists of two layers of fluid initially at rest in the gravity field in  $\Omega = ]-d/2, d/2[ \times ]-2d, 2d[$ . The initial data proposed in Reference [14] are as follows. The initial position of the interface is  $\eta(x) = -0.1d \cos(2\pi x/d)$ . The heavy fluid is above and the density ratio is 3, so that the Atwood number is 0.5 according to the definition  $A_t = (\rho_{\max} - \rho_{\min}) / (\rho_{\max} + \rho_{\min})$ . The transition between the two fluids is regularized by means of the following law:

$$\frac{\rho(x, y, t = 0)}{\rho_{\min}} = 2 + \tanh\left(\frac{y - \eta(x)}{0.01d}\right)$$

The governing equations are made dimensionless by using the following references:  $\rho_{\min}$  for density,  $d$  for length, and  $d^{1/2}g^{-1/2}$  for time, where  $g$  is the gravity field, so that the reference velocity is  $d^{1/2}g^{1/2}$ , and the Reynolds number is defined by  $Re = \rho_{\min}d^{3/2}g^{1/2}/\mu$ . Assuming the symmetry of the initial condition is maintained during the time evolution, the computational domain has been restricted to  $]0, d/2[ \times ]-2d, 2d[$ . A no-slip condition is enforced at the bottom and top walls while symmetry is imposed on the two vertical sides.

#### 3.2. On the inviscid limit of the RT instability

We made computations with finite elements and finite volumes at  $Re = 1000$  and  $5000$ . The aim of this study is to verify whether the problem considered has a limit solution as the Reynolds number increases to infinity, as suggested by the computations of Tryggvason [14].

The time evolution of the interface of the density field for  $Re = 1000$  is plotted in Figure 1 at times 1, 1.5, 1.75, 2, 2.25, 2.5 in the time scale of Tryggvason which is related to ours by  $t_{\text{Tryg}} = t\sqrt{A_t}$ . The finite volume solution is shown at the top of the figure and the finite element one is at the bottom. The finite volume mesh is composed of  $256 \times 512$  cells and the finite element mesh has 30189  $\mathbb{P}_2$  nodes. The two solutions are consistent in that they show similar structures and differ only in fine details at large time; the finite volume gives more details showing that it is twice as much refined as the finite element one.

To further assess the sensitivity of the method to spatial resolution and to verify that the artificial viscosity is much smaller than the physical one, we have solved the same problem

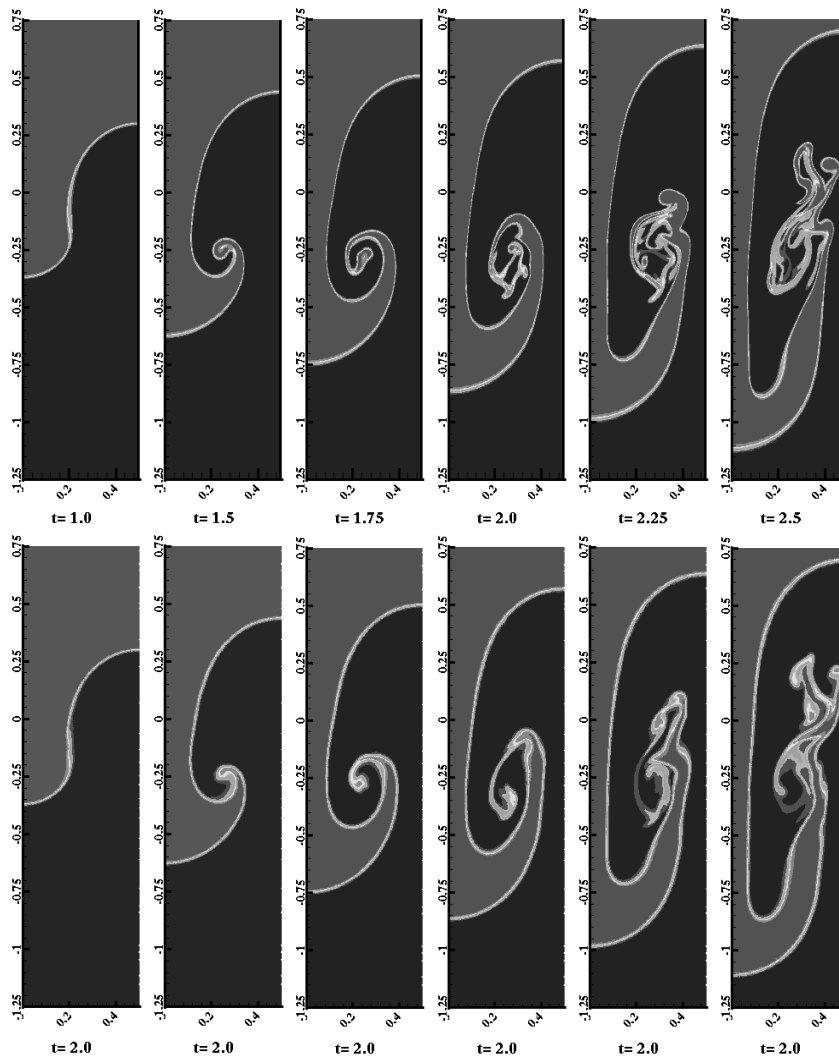


Figure 1.  $Re = 1000$ . Top, finite volumes,  $256 \times 512$  cells; bottom, finite elements, 30189  $\mathbb{P}_2$  nodes. The interface is shown at times: 1, 1.5, 1.75, 2, 2.25, and 2.5.

for  $Re = 5000$ . In Figure 2, we show the evolution of the interface computed using the same finite volume mesh as before and a finite element mesh composed of 49577  $\mathbb{P}_2$  nodes.

We compare now the viscous solutions,  $Re = 1000$  and 5000, with the inviscid one computed in Reference [14].

We first compare the position of the interface of the rising and falling bubbles as a function of time. The positions predicted by the finite element and the finite volume method for  $Re = 1000$  and 5000 are almost coincident and are in fair agreement with that reported in Reference [14]. We notice though that the velocity of the falling bubble is somewhat higher in our calculations than in Reference [14]. The computational domain used in Reference [14]

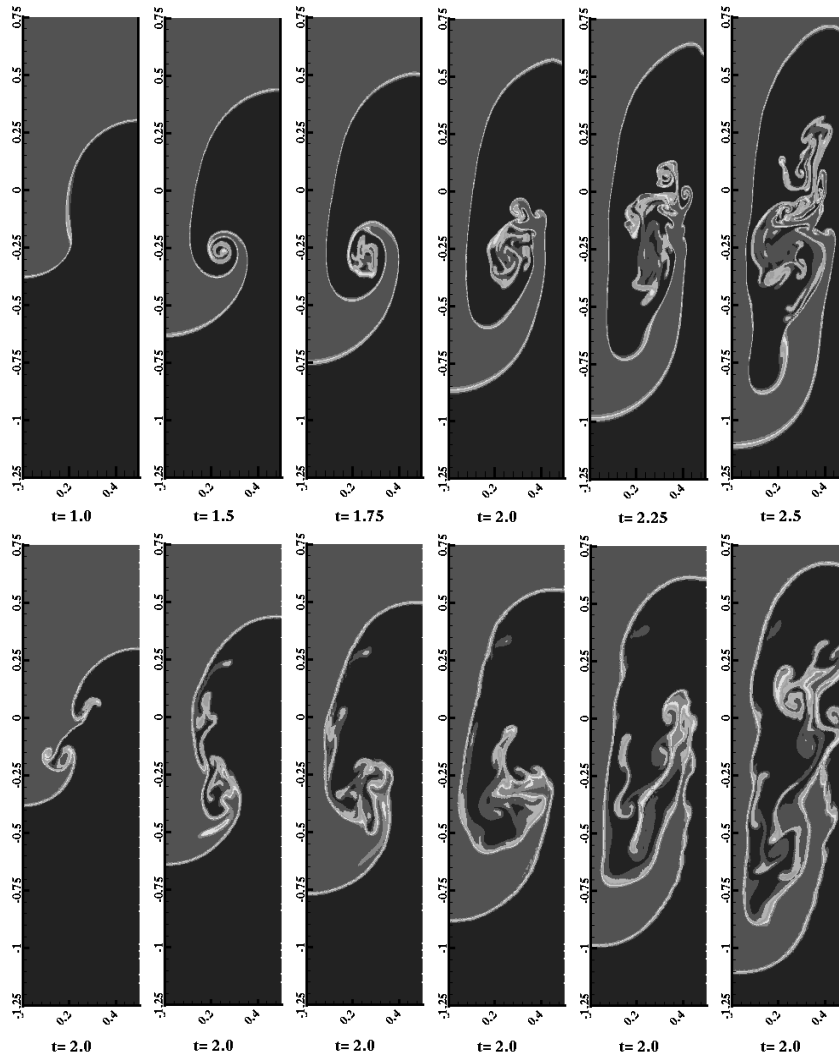


Figure 2.  $Re = 5000$ . Top, finite volumes,  $256 \times 512$  cells; bottom, finite elements, 49577  $\mathbb{P}_2$  nodes. The interface is shown at times: 1, 1.5, 1.75, 2, 2.25, and 2.5.

is  $\Omega = ] -d/2, d/2[ \times ] -d, d[$ ; as a result, the asymptotic velocity of the falling bubble in the inviscid simulation is reduced due to the presence of the lower no-through flow boundary. See [7] for detailed comparisons.

Coming to the comparison of the vortex structure, there is a satisfactory agreement of the global characteristics of the flow between the viscous solutions and the inviscid one [14, Figure 4], especially in the early stage; note, however, that the roll-up of the main vortex in the present calculation does not develop since the singularity at the centre of the vortex is removed by viscous dissipation.

All these results indicate that an accurate and detailed prediction of such a flow for times  $t \geq 1.5$  and  $Re \geq 5000$  is a difficult task. In any case, note that our finite element and finite volume  $Re = 5000$  solutions are so different from the inviscid one reported in Reference [14] that we face the question of knowing whether the infinite Reynolds limit of the viscous solution should be equal to the inviscid solution. In this respect, we recall that Birkhoff had speculated that the initial-value problem (for inviscid stratified flows) might be ill-posed (as a consequence of the fact that) the growth rate of an infinitely small unstable wave is proportional to the square root of its wave number, as reported by Tryggvason. Our results seem to confirm Birkhoff's conjecture in the sense that this problem has no smooth inviscid solution for large times.

### 3.3. Sensitivity with respect to the numerical scheme

In this section, we discuss the finite volume results obtained for the case  $Re = 5000$ . We compare Superbee and Super-C schemes. The results obtained with Super-C are shown in Figure 3. We observe similar evolutions of the interface up to  $t = 1.25$ . A slight difference in the spiral structure occurs at  $t = 1.5$ . Superbee produces a nearly perfect roll-up, while the spiralling motion is disrupted for Super-C. As a result, for the latter times, the instabilities grow differently, although the mean features bear some resemblance, and the breakdowns of the upwards structure occur approximately at the same location and at the same time ( $2 < t < 2.5$  and  $-0.2 < y < -0.1$ ).

Beyond  $t = 1.75$ , the flow of the heavy fluid is composed by a core trailing the falling bubble and an arm resulting from the breakdown of the roll-up motion. The core stretches under the action of the falling bubble, and the arm elongates upwards with instabilities growing at its end. The length of the upwards plume is identical in both cases.

In the Superbee case, the main source of instabilities seem located at the arm's extremity. The arm's end complex motion begins to disrupt the core's interface, slightly at  $t = 2.5$ . We note also that no instability develops along the external interface of the arm.

In the Super-C case, the instabilities seem to grow faster and the dynamics seems richer than in the Superbee case. The plume seems to be better resolved as it shows more long-winded and wrinkled structures. The interface undergoes Kelvin–Helmholtz-like instabilities along the arm. The complex dynamics induced by the instabilities generate waves along the core's interface.

The Super-C scheme, applied to the 2D problem considered here, seems to generate under-shoots and overshoots on the density that are more important than for the Superbee scheme. The overshoots and undershoots are mainly localized near interfaces and are typically of the order of 1 per cent. The most important values (about 3–5 per cent) are rare and are localized in the long-winded structures in the plume. In the Superbee case, the more diffusive effect of the scheme smooths the small structures. As a result, it reduces the number of undershoots and overshoots as well as their intensity, with maximum values of the order of 3 per cent that are very rare.

This comparative study emphasizes the influence of the schemes on the results. Choosing can be difficult. The two schemes that we used seemed to have good ability to enforce mass conservation with discontinuous initial data. However, they may be inaccurate when dealing with small structures. On the one hand, Superbee tends to smooth them too much due to diffusive effects. On the other hand, because of more compressive properties, we suspect that



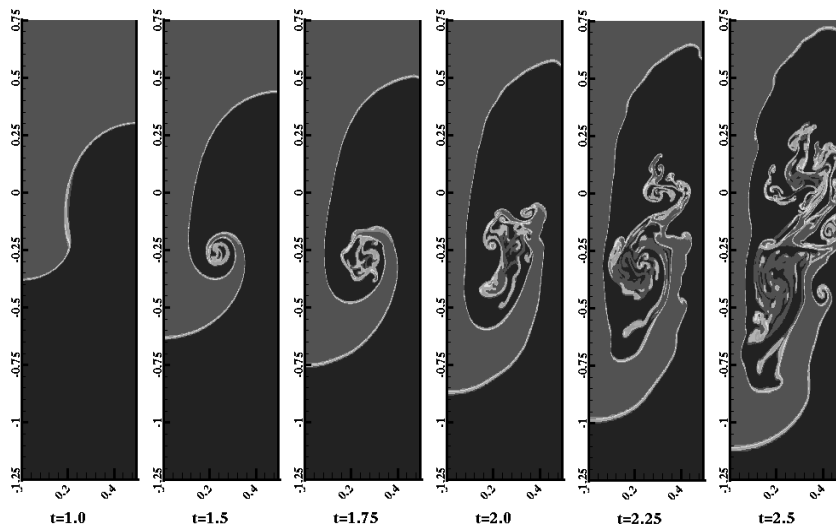


Figure 3.  $Re = 5000$ . Finite volume solution. The interface is shown at times: 1, 1.5, 1.75, 2, 2.25, and 2.5.

Super-C generates spurious structures by interaction between the grid and the fluid interface especially when its curvature is important. Note, however, that the problem is complex and more investigations are needed to sort out the origin of these shortcomings. Here, our purpose is only to show that for 2D Rayleigh–Taylor instabilities, there is a tremendous sensitivity of the approximate solution with respect to the choice of the numerical scheme.

#### 4. CONCLUSIONS

In this work, we have extended the projection method to the case of incompressible viscous flows with non-uniform density. A second-order unconditionally stable projection scheme has been proposed which is based on performing two projections per time step and using a three-level BDF scheme for the time integration of the mass conservation and momentum equations.

To verify the correctness of the method, it has been applied to a test case previously considered in the literature. The problem consists in simulating the evolution of the Rayleigh–Taylor instability of the interface between fluids of different densities. The results of the method in the range  $Re \approx 1000$  are in agreement with the inviscid computations [14] only in the early stages of vortex formation and roll-up.

By comparing the finite element solution to a finite volume one, we have come to the conclusion that the considered problem has no inviscid smooth limit, hence confirming a conjecture by Birkhoff stating that the inviscid problem is not well-posed for large times. Furthermore, we have shown that at even moderate Reynolds numbers, this problem is extremely sensitive to mesh refinement and to the numerical method adopted. This problem is a good test case for numerical methods dedicated to the solution of conservation laws.

## REFERENCES

1. Lions P-L. Mathematical Topics in Fluid Mechanics. In *Incompressible Models*, vol. 1. Oxford: Clarendon Press, 1996.
2. Chorin AJ. *Mathematical Computation* 1968; **22**:745–762.
3. Chorin AJ. *Mathematical Computation* 1969; **23**:341–353.
4. Temam R. Navier–Stokes Equations. In *Studies in Mathematics and its Applications*, vol. 2. Amsterdam: North-Holland, 1977.
5. Temam R. *Archive of Rational Mechanics and Analysis* 1969; **33**:377–385.
6. Bell JB, Marcus DL. *Journal of Computational Physics* 1992; **101**:334–348.
7. Guermond J-L, Quartapelle L. *Journal of Computational Physics* 2000; **165**:167–188.
8. Guermond J-L, Quartapelle L. *Journal of Computational Physics* 1997; **132**:12–33.
9. Guermond J-L. *Modélisation Mathématique et Analyse Numérique (M<sup>2</sup>AN)* 1999; **33**:1293–1316.
10. Leonard BP. *Computational Methods in Applied Mechanics and Engineering* 1991; **88**:17–74.
11. Vincet S, Caltagirone JP. *International Journal of Numerical Methods in Fluids* 1999; **30**:795–811.
12. Roe PL. In *Large Scale Computations in Fluid Mechanics, II*, Lectures in Applied Mathematics, vol. 22. Providence, RI: AMS 1985; 163–193.
13. Sweby PK. *SIAM Journal on Numerical Analysis* 1984; **21**:995–1011.
14. Tryggvason G. *Journal of Computational Physics* 1988; **75**:253–282.